International Journal of Mass Spectrometry 291 (2010) 61–66

Contents lists available at ScienceDirect

International Journal of Mass Spectrometry

journal homepage: www.elsevier.com/locate/ijms

Ionizing nonvolatile samples using laser desorption–proton-transfer reaction with cluster reagent ions

Chi-Wei Liang[a,b], Yuan Tseh Lee[a,b], Chung-Hsuan Chen[a,b], Yi-Sheng Wang[b,*]

[a] Department of Chemistry, National Taiwan University, Taipei 10617, Taiwan
[b] Genomics Research Center, Academia Sinica, 128, Academia Road, Section 2, Taipei 11529, Taiwan

ARTICLE INFO

Article history:
Received 15 August 2009
Received in revised form 11 January 2010
Accepted 19 January 2010
Available online 25 January 2010

Keywords:
Laser desorption
Proton-transfer reaction
Protonated cluster
Evaporative cooling
Carbohydrate

ABSTRACT

This work presents a novel chemical ionization method for producing intact molecular ions from nonvolatile samples. The ionization reaction combined the ejection of material by laser desorption (LD) and ionization by proton-transfer reactions (PTR) with protonated reagent clusters such as H^+/H_3^+, $H^+(H_2O)_n$, or $H^+(NH_3)_m$. The exoergicity of soft PTR was optimized using reagent cluster ions of appropriate proton affinities usually with high solvation numbers. The fragmentation of product ions was suppressed via thermalization with buffer gas or the evaporative cooling of the solvating molecules, and the protonated analyte–reagent complexes were obtained when low PTR exoergicity was achieved. The intact-to-fragment ratio of phenylalanine-glycine-glycine obtained by the LD-PTR roughly increased 28 times in comparison with that by MALDI. Protonated sucrose was also obtained with negligible fragments, although a harsh desorption condition was applied. The LD-PTR method allows the examination of neutral compositions produced in the LD process and facilitates the production of protonated analytes that cannot be obtained by conventional ionization strategies.

1. Introduction

For nonvolatile samples, electrospray ionization (ESI) [1] and matrix-assisted laser desorption/ionization (MALDI) [2] are two of the most well-established ionization methods. During these ionization reactions, many neutral analytes are liberated from the condensed phases into the gas-phase. The typical ion-to-neutral abundance ratio for peptide molecules in MALDI, as reported in the literature [3,4], is of the order of 10^{-5}. The ratio would be lower than 10^{-5} for carbohydrates because more substantial amount of carbohydrate samples are normally consumed to obtain a comparable spectral quality to that of the peptides. Therefore, post-ionization of the neutral compositions is expected to enhance the ion yield and reveal complementary sample information [5,6]. Many ionization strategies combine post-ionization processes subsequent to laser desorption (LD) such as LD photoionization (PI) [6,7], LD electron ionization (EI) [8], LD chemical ionization (CI) [9,10], and LD-electron attachment [11].

The production of intense analyte ions while minimizing fragmentation is key to post-ionization. PI is a convenient method, but the ionization efficiency depends strongly on the optical properties and the ionization energy (IE) of the analytes. Thus, PI normally produces fragments in multiphoton processes used to excite the analyte to a level above its IE. EI also produces extensive fragmentation because there is no efficient energy dissipation reaction involved. CI has the advantage over other methods because the dissociation of reagent molecules after the charge transfer reactions stabilizes the ionic analytes [12,13]. Take the proton-transfer reaction (PTR) as an example (Eq. (1)):

$$\text{Proton-transfer reaction} \quad A + MH^+ \rightleftharpoons AH^+ + M, \quad \Delta E_{PTR} \qquad (1)$$

where A represents the analytes, M the reagent molecules, and ΔE_{PTR} the exoergicity of the PTR reaction. The forward reaction occurs if the proton affinity (PA) of A exceeds that of M ($\Delta E_{PTR} < 0$), and the fragmentation of AH^+ may be reduced if $|\Delta E_{PTR}|$ is small. PTR mass spectrometry (MS) [14,15] is one of the well-established approaches that employs protonated molecules as reagent ions, normally with hydronium ions (H_3O^+). The principal feature of PTR is a long reaction time of the volatile organic compounds within ion swarms to obtain a very high sensitivity (in the pptv range) similar to that of flowing afterglow, flow drift tube, or selected ion flow tube devices [16–20]. However, fragmentation may still dominate the spectra if the analytes are fragile or the reaction exoergicity in Eq. (1) is high. For instance, the protonation of carbohydrates is known to be difficult even with soft ionization approaches such as ESI, MALDI, CI, and fast-atom bombardment.

The low ion yield of carbohydrates such as glucose mainly follows its low PA that makes the backward reaction of Eq. (1) favor-

* Corresponding author.
E-mail address: wer@gate.sinica.edu.tw (Y.-S. Wang).

1387-3806/$ – see front matter © 2010 Elsevier B.V. All rights reserved.
doi:10.1016/j.ijms.2010.01.010

Table 1
Proton affinity of commonly used molecules, biomolecules, and MALDI matrices.

Molecule		Proton affinity (kJ/mol)
Reagent gas	$(H_2O)_n$, $n=1$	702[a,b]
	$n=2$	828[b]
	$n=3$	882[b]
	$n=4$	911[b]
	$n=5$	924[b]
	$n=6$	945[b]
	$(NH_3)_x$, $x=1$	853[a,c]
	$x=2$	957[c]
	$x=3$	1028[c]
	$x=4$	1087[c]
	H_2	422[a]
Biomolecule	Arginine	1051[a]
	Phenylalanine	923[a]
	Glycine	887[a]
	Tryptophan	949[a]
	Glucose	819[d]
MALDI matrix	THAP	882[e]
	2,5-DHB	853[f]
	CHCA	841[g]

[a] (1) NIST Standard Reference Database Number 69—March 6, 2009 Release. (2) Ref. [22].
[b] Ref. [23].
[c] Ref. [21].
[d] Ref. [24].
[e] Ref. [27].
[f] Ref. [25].
[g] Refs. [26,28].

able. Table 1 lists the PA values of some reagent molecules [21–23], analytes [22,24], and commonly used MALDI matrices [25–28]. Two exceptions are the use of water monomer and hydrogen molecules as the reagent gas, but the PTR from these two molecules to glucose produces a large $|\Delta E_{PTR}|$ in Eq. (1) and further induces extensive dehydration reactions [29]. Another common observation is that only alkali metal ion attachments are present [30]. The difficulty in protonation makes the study of the gas-phase basicity of carbohydrates difficult; only the gas-phase basicity of glucose has been reported in the literature [24]. The suppression of fragmentation in PTR-MS requires suitable reagent ions to achieve the balance between reaction exoergicity and energy dissipation such as the reagent ion with a large heat capacity to redistribute the energy efficiently. An alternative approach involves the incorporation of additional energy dissipation reactions to stabilize the product ions.

This work demonstrates the combination of LD and the cluster-ion PTR method as an effective approach to produce protonated nonvolatile molecules, including phenylalanine-glycine-glycine (PGG), angiotensin I (Ang), and sucrose (Suc). Suppression of analyte fragmentation is achieved presumably by thermalization with buffer gas and the evaporative cooling process of the solvated molecules in the cluster. Although protonated clusters have been used to react with some volatile compounds [31–33], the use of ionic clusters as reagent ions of CI for laser-desorbed nonvolatile biomolecules has not been described before. The reagent cluster ions utilized in this work include H^+/H_3^+, $H^+(H_2O)_{1-6}$, or $H^+(NH_3)_{1-5}$. The energetics of the ionization reactions and the performance of the LD-PTR under various source conditions are discussed.

2. Experimental method

Experiments were conducted using a home-made linear time-of-flight (TOF) mass spectrometer equipped with a LD-PTR ion source. The reagent cluster ions were produced using a hollow cathode discharge (HCD) device [34,35]. The nonvolatile samples were desorbed into the high-density region of the reagent cluster ions for PTR, and the product ions were accelerated toward the TOF analyzer with various delays. The overall flight distance was roughly 1 m. Fig. 1 schematically depicts the HCD device and the ion optics.

The HCD device comprised a Pyrex cylinder, a hollow cathode assembly, and an anode tube. The Pyrex cylinder was selected for its low thermal expansion and shock-resistive properties. It was joined with the hollow cathode assembly to develop a discharge region of 55 mm i.d. and 82 mm long. The hollow cathode assembly was a metal disk of roughly 60 mm o.d. and 5 mm i.d., comprising a hexagonal-shaped hollow cathode fastened at the center of its discharge side and with a sample mount integrated into its vacuum side. The central orifice of the metal disk allowed the discharge gases and the reagent ions to co-expand toward the ion-optics region (Fig. 1). The discharge gases became the buffer gases when they came into the ion drift region. This orifice was covered by mesh with 88% transmittance (BM0090-01-N, InterNet, Minneapolis, MN) to generate a well-defined electric field.

The hexagonal hollow electrode was constructed by six metal sheets fastened on a stainless steel (S.S.) frame of 15 mm deep and 5 mm wide on every face. The non-cylindrical geometry allowed the easy replacement of clean metal sheets. The sample mount accommodated removable sample plates that were rectangular S.S. plates. Each sample plate comprised of a 2 mm hole that aligned coaxi-

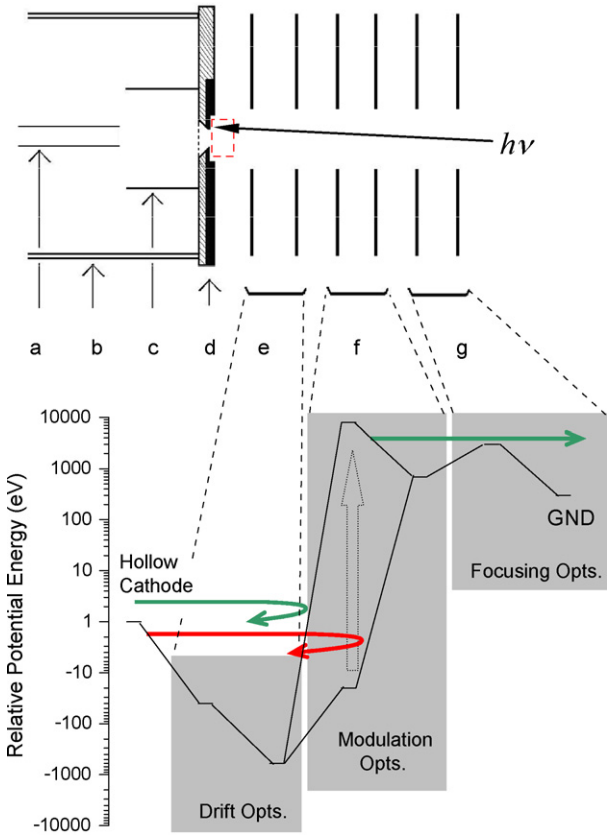

Fig. 1. Schematic of HCD device and relative electric potential for experiments. The HCD includes an anode tube (a), a dielectric cylinder (b), a hexagonal hollow cathode (c), and a metal disk (d) that accommodates removable sample plates (black colored). Lens-pairs e, f, and g are the ion-drift, modulation, and focusing optics, respectively. The red rectangular area denotes the PTR region. The reference of the potential energy diagram is the potential of the hollow cathode. In the retarding mode, the potential of the lens-pair f is low, and the ion trajectory is represented by the red line. In the extracting mode, the potential of the lens-pair f is high, and the ion trajectory is represented by the green lines. (For interpretation of the references to color in this figure legend, the reader is referred to the web version of the article.)

ally with the central orifice of the hollow cathode assembly when properly installed.

The anode tube was a grounded 1/8 in. S.S. tube that supplied the discharge gases and sustained the electric current for HCD. It was installed axially in the discharge region with its tip located 3 mm behind the central orifice of the hollow cathode assembly. The hollow cathode was kept constant at roughly −330 V for generating $H^+(H_2O)_{1-6}$. The typical current to sustain the plasma was 3 mA, corresponding to a power of roughly 1 W. The heat was dissipated via conduction to the vacuum chamber, making the temperature of the HCD device rose by less than 10 °C when the HCD was operated at 4 W for 30 min.

Discharge gases were premixed in a direct flow system and supplied to the HCD region using a leak valve. A glass bubbler was integrated into the flow system to accommodate the liquid discharge molecules such as water. This bubbler was sunk into a temperature-regulated water bath for the adjustment of the vapor pressure of the discharge liquid. To produce $H^+/H_3{}^+$, the discharge gas was 20% hydrogen in neon gas. To produce H_3O^+, $NH_4{}^+$, or $H^+(NH_3)_m$, the discharge gas was 25% water vapor, 20% ammonia in neon gas, or pure ammonia vapor, respectively. For such gaseous discharge molecules, a backing pressure of typically 90 mbar and a flow rate of 300–450 sccm were used. To produce $H^+(H_2O)_n$ with high solvation numbers, the discharge gas was pure water vapor with a backing pressure of roughly 23 mbar and a flow rate of 1200–1800 sccm. In all cases, the resultant pressure inside the HCD region and the source chamber was roughly 0.33–0.47 and 1.5×10^{-3} mbar, respectively.

The samples were deposited around the hole of the sample plates and desorbed by using a frequency-triplet Nd:YAG laser beam (355 nm, LS-2134UTF, Lotis TII, Minsk, Belarus). The laser beam was focused by a fused silica lens (f = 750 mm) and examined the sample surface at an incident angle of roughly 2° from the surface normal. The laser spot diameter was roughly 300 μm on the sample surface with typical laser irradiance of about 3000 J/m^2 for LD-PTR and 1800 J/m^2 for MALDI or LDI. The repetition rate of the laser was 5 Hz, and the mass spectra typically averaged 100 laser shots.

PTR proceeded in an ion drift region that was defined by the hollow cathode and two washer-shaped electrodes (lens-pair e in Fig. 1). The PTR region (red rectangular region in Fig. 1) was a few millimeters beyond the hollow cathode. Beyond the ion drift region, two additional sets of ion optics were installed to modulate the PTR duration (lens-pair f) in retarding or accelerating modes and to focus (lens-pair g) the ion beam, respectively. In the retarding mode, −20 V and +710 V with respect to the potential of HCD were applied respectively to the first and second electrode of the lens-pair f. Under the accelerating mode, a pulsed voltage of typically +6–13 kV was supplied to the first electrode of the lens-pair f to accelerate the ions toward the TOF analyzer, as depicted in the potential map of Fig. 1. The lens-pair g comprised of a d.c. biased and a grounded electrode to focus the ion beam. All electrodes were installed coaxially with a gap of 10 mm from the adjacent electrodes.

PGG, Ang, Suc and α-cyano-4-hydroxycinnamic acid (CHCA) were obtained commercially (Sigma-Aldrich, St. Louis, MO) and used without further purification. The analytes and the CHCA were each dissolved in 50% acetonitrile aqueous stock solutions with various concentrations. To prepare the PGG/CHCA sample, 1 μL of 0.05 M PGG solution was mixed with 5 μL of 0.05 M CHCA solution. One microliter of the above mixture was deposited uniformly around the hole of the sample plate. The same method and quantity were used to prepare the Suc/CHCA. The Suc/CHCA was also mixed with equal amount of pyridine as CHCA for comparison. To prepare Ang/CHCA, 1 μL of 0.005 M Ang solution was mixed with 3 μL of 0.05 M CHCA solution, and then 1 μL of this mixture was deposited to the sample plate. The samples were air dried on a heating plate (50 °C) for 1 min and vacuum-dried before conducting the measurements.

3. Results and discussion

3.1. LD-PTR involving reagent cluster ions

Protonated clusters exhibit three features that make them ideal reagent ions for PTR. First, the collision cross-section of the reagent cluster ions increases with cluster size, thus increasing the reaction probability [23,36]. Second, fragmentation of ions can be reduced considerably by a large number of vibrational degrees-of-freedom of the clusters, which redistribute the exoergicity efficiently. Third, energy dissipation of ion-neutral complexes can also occur via evaporative cooling, such as in the dissociation of non-covalent bonds of the molecular network (or desolvation reactions). The ionization reactions started while the reagent cluster ions collide with gaseous neutral analytes, presumably via ligand switching or association reactions [37–41]:

$$\begin{aligned} &\text{Ligand switching} \quad H^+(M)_n + A \rightarrow [H^+(M)_{n-1}A]^* + M, \quad \Delta E_{LS} \\ &\text{Association reaction} \quad H^+(M)_n + A \rightarrow [H^+(M)_n A]^*, \quad \Delta E_{Association} \end{aligned} \tag{2}$$

The ligand switching and association reactions are both exothermic. For biomolecules with high proton affinity, the ligand switching could be the dominant pathway. The excess energies of the complexes may be dissipated via thermalization with buffer gas or evaporative cooling (endothermic) processes as proposed in Eq. (3).

$$\begin{aligned} \text{Evaporative cooling} \quad [H^+(M)_n A]^* &\rightarrow [H^+(M)_{n-1}A]^* + M, \quad \Delta E_{D1} \\ &\rightarrow \dots \\ &\rightarrow [H^+(M)_{n-m}A]^* + m \cdot M, \quad \Delta E_{Dm} \end{aligned} \tag{3}$$

The evaporation of solvating molecules from large clusters is efficient because the dissociation energy normally decreases as the solvation number (n) increases [42]. The sequential evaporation of solvating molecules is favorable when $-\Delta E_{LS}$ or $-\Delta E_{Association}$ exceeds ΔE_{D1}, but fragmentation may persist if $-\Delta E_{LS}$ or $-\Delta E_{Association}$ is much higher than $\Sigma_n \Delta E_{Dn}$, that is, to eventually cause the cleavage of the weakest bond of AH^+. In contrast, incomplete desolvation may occur if large cluster ions are used, such as when $\Sigma_n \Delta E_{Dn}$ is higher than $-\Delta E_{LS}$ or $-\Delta E_{Association}$. The best condition for producing protonated analyte is when $\Sigma_n \Delta E_{Dn} \approx -\Delta E_{LS}$ or $-\Delta E_{Association}$. Under such condition, the fragmentation can be significantly suppressed with a trivial amount of reagent–analyte complexes.

The properties of the reagent cluster ions depended on the ion source condition. Protonated water clusters with n = 1–5 were normally obtained when using pure water vapor, as shown in Fig. 2a. Under this condition, the typical ion flux was about 1 μA/cm^2. The n shifted to higher distribution if the discharge gas pressure was increased, the sample temperature was lowered, or the discharge current was decreased. For pure ammonia, the observed maximum n and ion flux was normally 4 and 0.85 μA/cm^2, respectively (Fig. 2b). Lowering the ratio of the electric field strength (E) to the number density of buffer gas (N) in the ion drift region reduced the ion drift velocity v_d ($v_d = \mu E$, where μ is ion mobility) and the mean ion-neutral collision energy, as estimated by the method of McFarland et al. [43]. When E/N was 60 Townsend (Td), the mean collision energy of $H^+(H_2O)$, $H^+(H_2O)_2$, and $H^+(H_2O)_3$ toward heavy biomolecules at room temperature was about 0.05, 0.07, and 0.08 eV, respectively. If E/N was 120 Td, the values for $H^+(H_2O)$ and

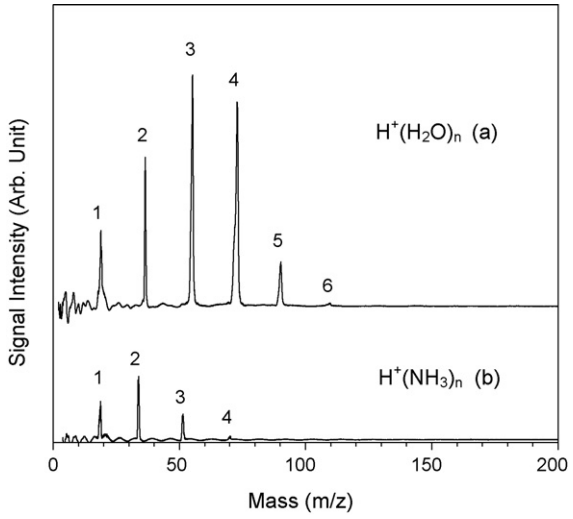

Fig. 2. Mass spectra of (a) protonated water cluster ions, $H^+(H_2O)_n$, and (b) protonated ammonia cluster ions, $H^+(NH_3)_n$, produced from HCD ion source with E/N of approximately 60–80 Td.

$H^+(H_2O)_2$ were 0.1 and 0.2 eV, respectively. The values of μ used to make these estimates were those associated with the drifting of ions in a nitrogen stream [43,44]. In this work, an E/N value of 60–80 Td was typically employed.

Most PTR reactive collisions were expected to occur within the PTR region because both densities of the LD-produced molecules and reagent ions were high. Fig. 3a–e shows the mass spectra of PGG/CHCA obtained using H^+/H_3^+, $H^+(H_2O)_n$, and $H^+(NH_3)_m$. The typical extraction delay used to obtain these spectra was 25–35 μs. The MALDI spectrum (Fig. 3f) obtained under optimal conditions when neither the discharge gas nor the reagent ions were flowing, shows abundant PGG fragment with $m/z = 121$ that corresponding to $[C_6H_5CH_2CHNH_2 + H]^+$. The use of a matrix was not a prerequisite for the LD process, but it markedly promoted molecular desorption due to the high optical density of the matrix. The direct LD of pure analytes was feasible for small molecules like tryptophan, but larger molecules could only be desorbed effectively when mixed with good photo-absorbing media such as matrices and graphite.

The temporal distributions of the intact and fragment ions of the PGG in LD-PTR were broad but clearly different from each other. Fig. 4 shows the ion intensities obtained by changing the extraction delays from 3 to 100 μs when reagent water clusters were used. The distribution of PGG fragment peaked at around 8 μs, whereas that of the protonated PGG peaked at around 25 μs. Notably, the ion signal shown roughly below 15 μs was produced directly in the laser desorption ionization (LDI) process, and the ions beyond 15 μs were produced by gas-phase PTR. The propagation of LDI ions was slow due to the resistance of the discharge gas flow and the absence of high acceleration voltages that are used in conventional MALDI-TOF instruments. The intact-to-fragment PGG abundance within 3–15 μs was 0.12 because the high desorption laser irradiance induced considerable fragmentation in LD process [45], similar to the result obtained in the MALDI mode (Fig. 3f). When the detectable signal was integrated over the entire range of extraction delays, the ratio was roughly 3.3. The increase of 27.5 times in the intact-to-fragment ratio was attributed to the low fragmentation in PTR beyond 15 μs.

When only the desorbed neutral molecules are considered, the quantity of analytes detected in LD-PTR MS can be estimated by [14,16]

$$[AH]^+ = [H^+(H_2O)_n]_0(1 - e)^{-k[A]t} \approx [H^+(H_2O)_n]_0[A]kt \quad (4)$$

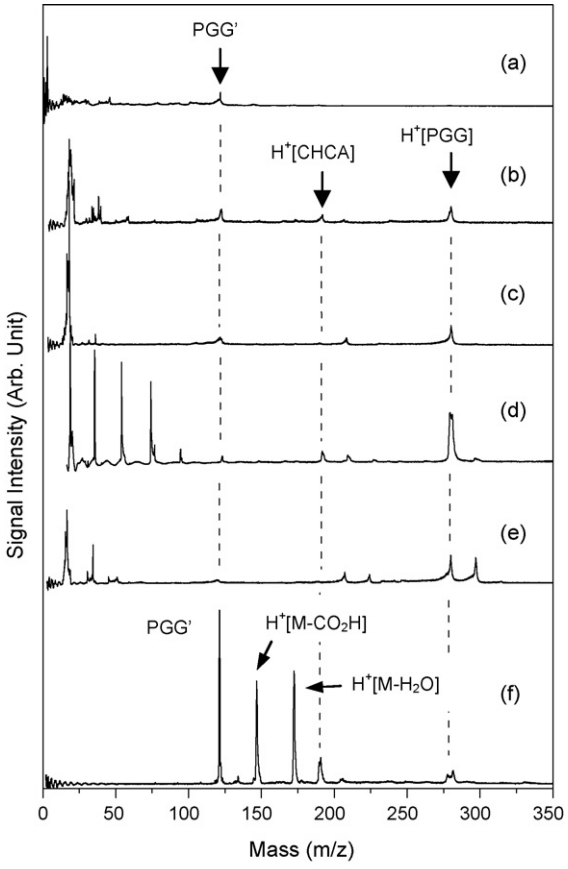

Fig. 3. Mass spectra of PGG/CHCA obtained using (a) H^+/H_3^+, (b) H_3O^+, (c) NH_4^+, (d) $H^+(H_2O)_n$, and (e) $H^+(NH_3)_n$ reagent ions in LD-PTR and using MALDI (f). PGG′ represents the important PGG fragment (121 m/z). The extraction delay used to obtain the MALDI spectrum was 2 μs. The spectrum shows PGG fragment (121 m/z), CHCA fragments (145 m/z and 172 m/z), protonated CHCA (190 m/z), and protonated PGG (280 m/z). The extraction delay in LD-PTR was 30 μs.

where $[H^+(H_2O)_n]_0$ represents the number density of reagent ions, k the reaction rate constant of PTR, and t the average time spent by the reagent ions in the PTR region. The diffusion losses of reagent and analyte ions were assumed to be low because a short drift length (~3 cm) was used. In this work, the $[AH^+]/[H^+(H_2O)_n]_0$ ratio

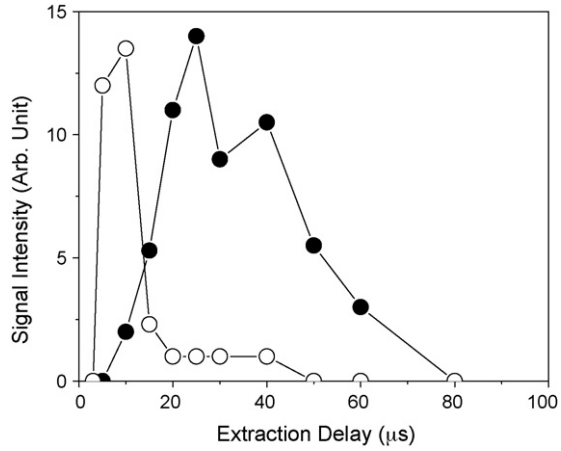

Fig. 4. Time evolution of protonated and fragment PGG signal in LD-PTR modes. The PGG fragment peaked at 8 μs and that of protonated PGG at 25 μs. The ions produced directly by the LD process are presumably present before 15 μs, and those produced by PTR are present after 15 μs. The E/N used in this experiment was approximately 70 Td. (○) PGG fragment (121 m/z); (●) protonated PGG (280 m/z).

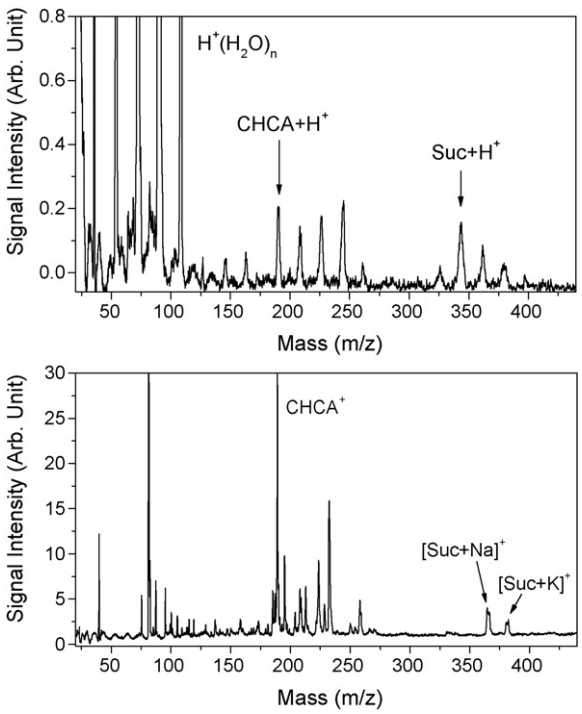

Fig. 5. Mass spectra of Suc obtained using LD-PTR of Suc/CHCA (a) and using MALDI with Suc/CHCA/pyridine. The *E*/*N* used in LD-PTR was 70 Td. Features to the right of the protonated CHCA and Suc in LD-PTR are solvated complexes. Small features at 325, 163, and 145 correspond to the fragments of Suc.

was obtained from the intensity of the corresponding spectral features (n = 1–6), and t was estimated to be 2.5 μs by dividing the length of the PTR region (5 mm) by the mobility of the reagent ions [44]. If using the k of acetone [36] and dimethylsulfoxide [31] in Eq. (4), a detection limit of better than 5 femtomole of analytes within the PTR region is obtained. Although k is not available for most biomolecules, the detection limit of biomolecules should be better because a higher k value is expected due to their larger dipole moments [46,47] and slower drift velocities [48].

3.2. LD-PTR of PGG, angiotensin I, and sucrose

As mentioned previously, large reagent clusters provide better energy dissipation efficiency than small reagent ions for suppressing fragmentation. When H^+/H_3^+ was used for the PGG/CHCA, the only feature associated with PGG was the fragment at m/z = 121 (Fig. 3a). Adjusting the discharge and the ion drift condition did not promote the appearance of the intact H^+[PGG]. The H^+[PGG] appeared only when protons were carried by water, ammonia, or their clusters (Fig. 3b–e). For example, using H_3O^+ for PTR produced comparable H^+[PGG] intensity as the PGG fragment (Fig. 3b). Fig. 3b also shows a small feature of H^+[CHCA] that is not presented in Fig. 3a. Using NH_4^+ as the reagent ion produced a similar result (Fig. 3c) as that of using H_3O^+, except that a small $H^+[CHCA + NH_3]$ feature seemed to replace the feature of protonated CHCA in Fig. 3b. The $H^+[CHCA + NH_3]$ is likely produced by the association reaction between NH_4^+ and CHCA, which is one of the primary process proposed in Eq. (2). This result was expected because the PA of CHCA exceeded that of H_2O but was lower than that of NH_3, so the proton was localized on NH_3 if $H^+[CHCA + NH_3]$ dissociate.

When $H^+(H_2O)_{1-6}$ were used in PTR, the feature of H^+[PGG] dominated the spectrum (Fig. 3d). A comparison with Fig. 3b shows that the improvement in the H^+[PGG] yield in Fig. 3d is very pronounced. Fig. 3d also shows noticeable water adducts on H^+[CHCA] and a small feature of $H^+[PGG + H_2O]$, suggesting that the water molecules did not fully evaporate upon PTR. The sharp reduction in the amount of fragments and the presence of reagent–analyte complexes indicate that both the collision energy and the exoergicity were low. Such complexes cannot survive in the harsh environments of MALDI, especially when high desorption laser irradiance is used. They are also rarely present in the mass spectra obtained using ESI. This result suggests that the LD-PTR with cluster ions is a very soft ionization strategy.

Reagent–analyte complexes were also present when $H^+(NH_3)_{1-3}$ were used (Fig. 3e), and the $H^+[PGG + NH_3]$ complex was as abundant as the H^+[PGG]. The sum of the intensities of H^+[PGG] and $H^+[PGG + NH_3]$ in this condition was roughly equal to the intensity of H^+[PGG] in Fig. 3d. In comparison with the result using NH_4^+ reagent ion, the yield of H^+[PGG] when using $H^+(NH_3)_{1-3}$ is greatly improved, and the $H^+[CHCA + 2NH_3]$ is also present in the spectrum. Because $H^+(NH_3)_{1,2}$ and $H^+[CHCA + (1,2)NH_3]$ respectively dominated the reagent cluster ions and the product ions, the association reaction was likely involved in the ionization process. On the other hand, the intensity of $H^+[PGG + H_2O]$ is much weaker than the $H^+[PGG + NH_3]$ because the PA of H_2O is 151 kJ/mol lower than NH_3. The lower dissociation energy of H_2O compared with NH_3 enhances the appearance of H^+[PGG], making water clusters better reagent ions than ammonium clusters.

This ionization strategy is advantageous for detecting fragile molecules like carbohydrates. The spectrum of Suc obtained using reagent water clusters included a favorable protonated feature and solvated complexes of up to three water molecules (Fig. 5a). The presence of protonated Suc–water complexes was due to the low PA of Suc, which made the exoergicity insufficient to fully evaporate the solvating water molecules. The small features with m/z of 325, 163, and 145 possibly corresponded to the laser-induced sucrose fragments of –OH, $-C_6H_{11}O_6$, and $-[C_6H_{11}O_6 + H_2O]$, respectively. Notably, no contamination of alkali metal adducts was detected with long extraction delay, such as >30 μs. Fig. 5b shows the spectrum of Suc/CHCA/pyridine obtained by MALDI. Mixing pyri-

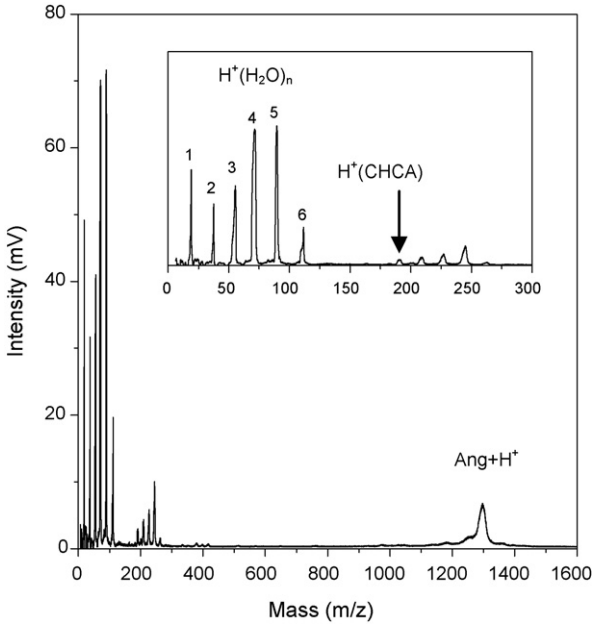

Fig. 6. LD-PTR mass spectrum of Ang/CHCA obtained using $H^+(H_2O)_n$ (n = 1–6) reagent ions. The *E*/*N* and the extraction delay were 70 Td and 30 μs, respectively. Inset shows the features in the reagent ion and matrix ion regions.

dine and CHCA formed ionic liquid matrix that improved the ion yield [49], but no protonated Suc was detected. The absence of protonated Suc in MALDI is presumably due to the competition of the matrix on the surface. Such competition is not important when protonation occurs in the gas-phase, as in the case of LD-PTR.

The reagent water clusters are appropriate for the ionization of proteins. Fig. 6 displays the mass spectrum of Ang obtained using reagent water clusters. The PTR condition used in this measurement was the same as that for Suc, as can be seen in the same distribution of protonated water–CHCA complexes in Fig. 5a. Protonated Ang was present in the spectrum without noticeable fragments or reagent–analyte complexes, suggesting that the $-\Delta E_{LS}$ or $-\Delta E_{Association}$ of Ang with the reagent water clusters is roughly the same as that with $\Sigma_n \Delta E_{Dn}$. The insets display the features of reagent water clusters and protonated water–CHCA complexes. In this case, the most abundant reagent ions were $H^+(H_2O)_4$ and $H^+(H_2O)_5$. These two cluster sizes were previously found to be the most reactive with acetone and dimethylsulfoxide among the sizes of $n = 1$–6 [23,36]. Under this condition, the cluster size of protonated water–CHCA complexes was up to $n = 3$, suggesting that the association energy of CHCA with these reagent ions ($n = 1$–6) was probably close to the evaporation energy of about two water molecules. This result qualitatively agrees with the result of previous kinetic measurements [42].

4. Conclusion

LD-PTR involving reagent cluster ions is a soft ionization method for nonvolatile biomolecules. Although the intense desorption laser irradiance produced extensive fragmentation to the sputtered ions, the abundant neutral compositions were mostly gaseous intact molecules that were suitable for subsequent PTR. In addition to the thermalization with buffer gas, the use of the reagent cluster ions in PTR facilitates the reduction of fragmentation by reducing exoergicity and incorporating the evaporative cooling mechanism. Thus, increasing desorption laser irradiance is advantageous for the soft PTR because more neutral analytes can be produced to enhance the signal intensity compared with the low laser irradiance. With the desorption condition used in this work, the spectrum of PGG/CHCA obtained using the direct LDI method shows an intact-to-fragment ratio of PGG ions of approximately 0.12. This ratio improves by 27.5 times if the PTR is utilized. Pure LD-PTR spectra were obtained with an extraction delay of above 15 μs after the desorption laser. The LD-PTR not only allows the diagnosis of neutral compositions produced in MALDI and LD but also facilitates the protonation of analytes with low PA values. Protonated Suc can be routinely produced without the contamination of alkali metal adducts. The soft ionization characteristics of LD-PTR are also evident through the presence of protonated analyte–reagent complexes in the spectra of PGG and Suc. Based on this method, measurements of the gas-phase acidity and basicity of carbohydrates are currently under investigation.

Acknowledgments

The authors would like to thank the Genomics Research Center, Academia Sinica, and the National Science Council of Taiwan (Contract no. NSC 98-2113-M-001-021-MY3) for financially supporting this research.

References

[1] J.B. Fenn, M. Mann, C.K. Meng, S.F. Wong, C.M. Whitehouse, Science 246 (1989) 64.
[2] M. Karas, F. Hillenkamp, Anal. Chem. 60 (1988) 2299.
[3] A.P. Quist, T. Huthfehre, B.U.R. Sundqvist, Rapid Commun. Mass Spectrom. 8 (1994) 149.
[4] A.A. Puretzky, D.B. Geohegan, Appl. Surf. Sci. 129 (1998) 248.
[5] C.D. Mowry, M.V. Johnston, J. Phys. Chem. 98 (1994) 1904.
[6] B. Spengler, U. Bahr, M. Karas, F. Hillenkamp, Anal. Instrum. 17 (1988) 173.
[7] D.W. Beekman, T.A. Callcott, S.D. Kramer, E.T. Arakawa, G.S. Hurst, E. Nussbaum, Int. J. Mass Spectrom. Ion Process. 34 (1980) 89.
[8] J. Berkowitz, W.A. Chupka, J. Chem. Phys. 40 (1964) 2735.
[9] R.J. Cotter, Anal. Chem. 52 (1980) 1767.
[10] R.J. Perchalski, R.A. Yost, B.J. Wilder, Anal. Chem. 55 (1983) 2002.
[11] O. Ingolfsson, A.M. Wodtke, J. Am. Soc. Mass Spectrom. 12 (2001) 1339.
[12] J.H. Gross, Mass Spectrometry: A Textbook, Springer, Berlin; New York, 2004, pp. xviii.
[13] A.G. Harrison, Chemical Ionization Mass Spectrometry, CRC Press, Boca Raton, FL, 1983, p. 156.
[14] A. Hansel, A. Jordan, R. Holzinger, P. Prazeller, W. Vogel, W. Lindinger, Int. J. Mass Spectrom. 149/150 (1995) 609.
[15] W. Lindinger, A. Hansel, A. Jordan, Int. J. Mass Spectrom. 173 (1998) 191.
[16] J.H. Futrell, Gaseous Ion Chemistry and Mass Spectrometry, Wiley, New York, 1986, pp. xii, University of Utah. Dept. of Chemistry.
[17] M. McFarland, W. Lindinger, D.L. Albritton, Bull. Am. Phys. Soc. 20 (1975) 239.
[18] D. Smith, N.G. Adams, in: M.T. Bowers (Ed.), Gas Phase Ion Chemistry, Academic Press, New York, 1979.
[19] D.K. Bohme, Int. J. Mass Spectrom. 200 (2000) 97.
[20] D. Smith, P. Spanel, Mass Spectrom. Rev. 24 (2005) 661.
[21] J.D. Payzant, Cunningh Aj, P. Kebarle, Can. J. Chem. Rev. Can. Chim. 51 (1973) 3242.
[22] E.P.L. Hunter, S.G. Lias, J. Phys. Chem. Ref. Data 27 (1998) 413.
[23] Y. Kawai, S. Yamaguchi, Y. Okada, K. Takeuchi, Y. Yamauchi, S. Ozawa, H. Nakai, Chem. Phys. Lett. 377 (2003) 69.
[24] K.A. Jebber, K. Zhang, C.J. Cassady, A. ChungPhillips, J. Am. Chem. Soc. 118 (1996) 10515.
[25] R.D. Burton, C.H. Watson, J.R. Eyler, G.L. Lang, D.H. Powell, M.Y. Avery, Rapid Commun. Mass Spectrom. 11 (1997) 443.
[26] T.J.D. Jorgensen, G. Bojesen, H. Rahbek-Nielsen, Eur. J. Mass Spectrom. 4 (1998) 39.
[27] K. Breuker, R. Knochenmuss, R. Zenobi, Int. J. Mass Spectrom. 184 (1999) 25.
[28] S.P. Mirza, N.P. Raju, M. Vairamani, J. Am. Soc. Mass Spectrom. 15 (2004) 431.
[29] J.F. Gal, P.C. Maria, E.D. Raczynska, J. Mass Spectrom. 36 (2001) 699.
[30] M.A. Posthumus, P.G. Kistemaker, H.L.C. Meuzelaar, M.C. Tennoeverdebrauw, Anal. Chem. 50 (1978) 985.
[31] J.M. Thomas, A.A. Viggiano, J. Phys. Chem. A 103 (1999) 2720.
[32] T. Schindler, C. Berg, G. Niednerschatteburg, V.E. Bondybey, Chem. Phys. Lett. 229 (1994) 57.
[33] D. Smith, P. Spanel, Int. Rev. Phys. Chem. 15 (1996) 231.
[34] W. Lindinger, Phys. Rev. A 7 (1973) 328.
[35] A. Vizir, E.M. Oks, M.C. Salvadori, F.S. Teixeira, I.G. Brown, Rev. Sci. Instrum. 78 (2007) 086103.
[36] Y. Kawai, S. Yamaguchi, Y. Okada, K. Takeuchi, Int. J. Mass Spectrom. 220 (2002) 375.
[37] N.G. Adams, D.K. Bohme, D.B. Dunkin, F.C. Fehsenfe, E.E. Ferguson, J. Chem. Phys. 52 (1970) 3133.
[38] J.W. Larson, T.B. Mcmahon, J. Am. Chem. Soc. 105 (1983) 2944.
[39] G. Bouchoux, J.Y. Salpin, D. Leblanc, Int. J. Mass Spectrom. Ion Process. 153 (1996) 37.
[40] F. Dhooghe, C. Amelynck, J. Rimetz-Planchon, N. Schoon, F. Vanhaecke, Int. J. Mass Spectrom. 285 (2009) 31.
[41] D.K. Bohme, in: G. Tranter, J.C. Lindon, J.L. Holmes (Eds.), Encyclopedia of Spectroscopy and Spectrometry, Academic Press, 2000, p. 984.
[42] Y.-S. Wang, C.-H. Tsai, Y.T. Lee, H.-C. Chang, J.C. Jiang, O. Asvany, S. Schlemmer, D. Gerlich, J. Chem. Phys. A 107 (2003) 4217.
[43] M. McFarland, D.L. Albritton, F.C. Fehsenfeld, E.E. Ferguson, A.L. Schmeltekopf, J. Chem. Phys. 59 (1973) 6620.
[44] H.W. Ellis, E.W. McDaniel, D.L. Albritton, L.A. Viehland, S.L. Lin, E.A. Mason, Atom. Data Nucl. Data Tables 22 (1978) 179.
[45] S. Bourcier, S. Bouchonnet, Y. Hoppilliard, Int. J. Mass Spectrom. 210 (2001) 59.
[46] T. Su, W.J. Chesnavich, J. Chem. Phys. 76 (1982) 5183.
[47] S. Takashima, Biophys. Chem. 58 (1996) 13.
[48] L. Keck, U. Oeh, C. Hoeschen, Int. J. Mass Spectrom. 264 (2007) 92.
[49] M. Zabet-Moghaddam, E. Heinzle, A. Tholey, Rapid Commun. Mass Spectrom. 18 (2004) 141.